Analysis of thermally stratified flow of Sutterby nanofluid with zero mass flux condition

Saif-ur-Rehman[a,b],Nazir A. Mir[a],M. Farooq[a]

[a]Department of Mathematics and Statistics, Riphah International University, Islamabad 44000, Pakistan

[b]Department of Mathematics, COMSATS University, Islamabad 44000, Pakistan

Abstract: Stratification plays vital role in chemical process, oceanography, agriculture and geophysical flows. When two fluids with different temperatures are mixed, a density difference is generated and thermal stratification is induced between two fluids. Thermal stratified flows exist in single phase and multi-phase flows. Due to temperature differences, different layers of the fluid are generated . In nature, stratification process controls the oxygen and hydrogen ratio which controls species growth rate in lakes and ponds. Therefore, in this attempt, we scrutinizes the effects of Sutterby nanoliquid flow deformed by a linearly stretchable sheet. Inclined magnetic field is included to explore the features of electrically conducting fluid. Thermal stratification phenomenenon is implemented over a horizontal sheet to elaborate the features of heat transfer. Variable fluid features is also accounted. Zero mass flux condition is also incorporated along with Brownian diffusion and thermophoresis phenomenon. Using the suitable transformations, the system of partial differential equations are transmuted into coupled system of ordinary differential equations. Analytically solutions are computed via homotopic approach. Graphical behavior of applicable parameters on temperature, velocity, and concentration fields are illustrated and elaborated. Skin friction coefficient and Nusselt number are computed and analyzed.

Key-words: Sutterby fluid; Nanofluid; Thermal stratification; Variable thermal conductivity; Inclined MHD; zero mass flux condition.

1 Introduction

Nanoparticles are emerged into base fluid to form nanofluids. The nanofluids were initially named by Choi [1]. The nanoparticles (like metal, graphene, metal oxide, CNT etc.) are added in base fluid (i.,e., glycol, water, ethylene etc.) in order to enhance the fluid features like thermal conductivity. Nanoparticle's motion leads to thermal diffusion which depicts the nanofluid behavior. It is well recognized that nanoparticles are added to generate heat transfer media with conductivity of metals. Therefore, nanofluids are exercised in order to improve the efficiency of thermal devices. Fluid cooling and heating processes are significant in industries including power generation, engines, solar water heater, manufacturing, transportation, geothermal systems, heat pipes, electronic devices and nuclear reactors. In the view of its importance, Prasad et al. [2] described the radiative nanofluid flow under magnetic field. Tian et al. [3] discussed the convectively heated non-Newtonian magneto nanofluid flow past a stretchable sheet towards stagnation region. Ahmed et al. [4] explored the heat source features in Maxwell stagnant nanofluid over a rotating porous disk. Khan et al. [5] discussed the irreversibility aspect in Carreau nanofluid flow. Derakhshan et al. [6] explored the hydro-magneto analysis in nanofluid flow through parallel sheets.

Thermal conductivity is one of the variable property of fluids. It depends linearly or exponentially upon temperature. The temperature dependent thermal conductivity is incorporated to predict the heat transfer rate accurately. It has key role in industrial processes involving heat transfer. The scheme designed for materials having constant thermal conductivity is not suitable for variable fluid properties. Thermal coductivity involves in various research domains e.g. electronics, building insulation and many others. The materials (i.e. silver, copper, aluminium etc.) having high thermal conductance are utilized in turbines and electronic devices while low thermal conductivity materials (e.g. aluminia, polystyrene

etc.) are engaged in furnaces and building construction. Hamid et al. [7] explained the varying thermal features in Williamson magneto nanofluid flow considering mixed convection phenomenon. Hayat et al. [8] depicted the variable thermal conductivity analysis in hydromagneto stratified third grade fluid flow through stretched surface. Salawu et al. [9] illustrated the effect of varying conductivity in hydromagnetic radiative and reactive Powell-Eyring material flow saturated in porous media with entropy generation. Ahmed et al. [10] elaborated the variable conductivity analysis in Maxwell MHD fluid flow deformed by rotating disks. Khan et al. [11] addressed the variable fluid characteristics and irreversibility analysis in slip flow of radiative fluid considering mixed convection.

Process of stratification occurs in different natural and industrial domain. Variations in temperature with different fluid densities leads to the stratification process. It plays significant role in managing and controlling the ratio of hydrogen element and oxygen in the surroundings, which affects the rate of growth of diverse species. It involves in many processes like in agriculture field, volcanic flow systems, and also in rivers and reservoirs, usage of heterogeneous mixtures in food industries and density stratification of atmosphere. Bilal et al. [12] reported the magneto-hydrodynamic analysis of thermally stratified Carreau fluid flow. Anjum et al. [13] explored the slip features in stratified stagnant fluid flow deformed by Riga plate of varying thickness. Khan et al. [14] described the dual stratified Maxwell fluid flow with varying viscosity. Hamid et al. [15] explored the mixed convective double stratified Williamson nanofluid flow. Ali et al. [16] discussed the stratification analysis in Maxwell nanomaterial flow through inclined surface.

Main objective here is to investigates the variation of inclined magnetic strength on the flow of thermally stratified Sutterby nanofluid. Brownian diffusion and thermophoresis effects are considered. Thermal conductivity subject to temperature is also incorporated in current

analysis. zero mass flux condition is accounted at the boundary. Similarity variables are exercised to express the governing equations into dimensionless form. Homotopic technique (HAM) $[17-21]$ is adopted to acquire the approximate analytic solutions of the system. The influence of the involved parameters on temperature, velocity and fluid concentration is explored graphically. Furthermore, Nusselt number and drag force are analyzed explicitly.

2 Problem Formulation

The flow of incompressible Sutterby nanofluid past a stretching non porous sheet is analyzed. The inclined magnetic strength B_0 is incorporated in flow regime which makes an angle of α_1 with stretching sheet. The Cartesian coordinate system is chosen for the flow analysis as shown in Fig.1. Thermal stratification and varying thermal conductivity are considered. The heat and mass is subjected to zero mass flux condition. Fluid temperature T is assumed to be very large as compared to the ambient temperature T_∞. i.e $T_\infty << T$.

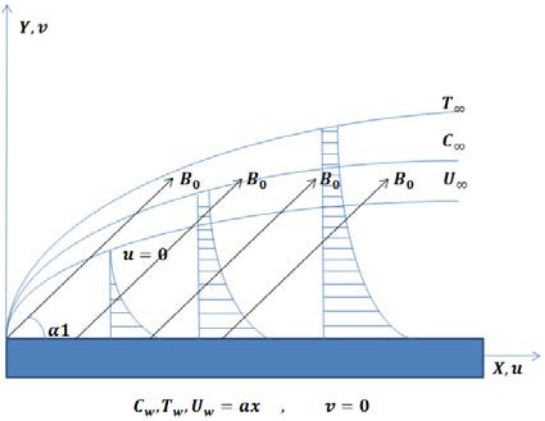

Fig.1 Flow geometry

Under boundary layer assumption, the standard equations take the form:

$$\frac{\partial u}{\partial x}+\frac{\partial v}{\partial y}=0, \tag{1}$$

$$u\frac{\partial u}{\partial x}+v\frac{\partial u}{\partial y}=\nu\left(1-\frac{\beta^2}{6}\frac{\partial u}{\partial y}\right)^n\frac{\partial^2 u}{\partial y^2}-\frac{n\nu\beta^2}{6}\left(1-\frac{\beta^2}{6}\frac{\partial u}{\partial y}\right)^{n-1}\frac{\partial u}{\partial y}\frac{\partial^2 u}{\partial y^2}-\frac{\sigma B_0^2\sin^2\alpha_1}{\rho}u, \tag{2}$$

$$\left(u\frac{\partial T}{\partial x}+v\frac{\partial T}{\partial y}\right)=\frac{1}{\left(\rho c_p\right)_f}\frac{\partial}{\partial y}\left(\kappa\left(T\right)\frac{\partial T}{\partial y}\right)+\frac{\left(\rho c_p\right)_{np}}{\left(\rho c_p\right)_f}\left(D_B\frac{\partial C}{\partial y}\frac{\partial T}{\partial y}+\frac{D_T}{T_\infty}\left(\frac{\partial T}{\partial y}\right)^2\right), \quad (3)$$

$$u\frac{\partial C}{\partial x}+v\frac{\partial C}{\partial y}=D_B\frac{\partial^2 C}{\partial y^2}+\frac{D_T}{T_\infty}\frac{\partial^2 T}{\partial y^2}, \quad (4)$$

with the boundary conditions:

$$\begin{aligned} u &= U_w\left(x\right)=ax,\ v=0,\ T=T_w\left(x\right)=T_0+bx,\ D_B\frac{\partial C}{\partial y}+\frac{D_T}{T_\infty}\frac{\partial T}{\partial y}=0 \ \ at\ y=0, \\ u &= 0,\ \ T=T_\infty\left(x\right)=T_0+b_1x,\ \ C\ \rightarrow\ C_\infty\ , \text{as } y\rightarrow\infty. \end{aligned} \quad (5)$$

Here u and v represent velocity components along the coordinate axes, ν represents fluid kinematic viscosity, β represents Sutterby fluid coefficient, ρ_f and ρ_{np} represent the densities of fluid and nanoparticles, n represents power law index, σ represents electrical conductivity, B_0 represents strength of constant magnetic field, α_1 represents inclination of the magnetic field , T represents the temperature of fluid, T_∞ represents free stream temperature, T_0 represents reference temperature, T_w represents wall temperature, c_{pf} and c_{np} represent heat capacities of the surface and nanoparticles, C represents concentration, D_B and D_T represent Brownian diffusion and thermal diffusion coefficients respectively, $U_w\left(x\right)=ax$ represents stretching velocity, a , $b, b1$ represent dimensional constants. The variable thermal conductivity $\kappa\left(T\right)$ satisfies the relation as:

$$\kappa\left(T\right)=\kappa_\infty\left(1+\epsilon\theta\left(\eta\right)\right), \quad (6)$$

κ_∞ and ϵ represent surrounding and dimensionless thermal conductivity respectively.

Utilizing the similarity transformations:

$$\psi = \sqrt{a\nu}f(\eta),\ \eta=\sqrt{\frac{a}{\nu}}y, \quad (7)$$

$$u = axf'(\eta),\ \upsilon=-\sqrt{a\nu}f(\eta), \quad (8)$$

$$\theta\left(\eta\right)=\frac{T-T_\infty}{T_w-T_0},\ \phi\left(\eta\right)=\frac{C-C_\infty}{C_w-C_0}, \quad (9)$$

the mass flux condition (1) is automatically satisfied while Eqs.(2-4) become:

$$\left(1-\frac{\alpha}{6}f''(\eta)\right)^{n}f'''(\eta)-\frac{n\alpha}{6}\left(1-\frac{\alpha}{6}f''(\eta)\right)^{n-1}f''(\eta)f'''(\eta)+f(\eta)f'(\eta)-(f'(\eta))^{2}-Mf'(\eta)\sin^{2}\alpha_{1}=0, \tag{10}$$

$$\theta''(\eta)(1+\epsilon\theta(\eta))+\epsilon\theta'(\eta)+\Pr\left(N_{T}\theta'(\eta)^{2}+N_{B}\varphi'(\eta)\theta'(\eta)+f(\eta)\theta'(\eta)-s1f'(\eta)-f'(\eta)\theta(\eta)\right)=0, \tag{11}$$

$$\varphi'(\eta)+\frac{N_{T}}{N_{B}}\theta'(\eta)+\Pr Lef(\eta)\varphi'(\eta)=0. \tag{12}$$

The associated boundary conditions take the form:

$$f(0)=0,\quad f'(0)=1,\quad f'(\infty)=0, \tag{13}$$

$$\theta(0)=1-s1,\ \theta(\infty)=0, \tag{14}$$

$$N_{B}\varphi'(0)+\ N_{T}\theta'(0)\ =0,\ \phi(\infty)=0, \tag{15}$$

here α represents fluid parameter, M represents Hartman number, Pr represents Prandtl number, Le represents lewis number, $s1$ represents thermal straitified parameter, N_B represents Brownian motion parameter, N_T represents thermosphoresis parameter. These quantities are defined through the following expressions:

$$\begin{aligned}\alpha &= \beta^{2}x\sqrt{\frac{a^{3}}{\nu}},\ \Pr=\frac{\mu c_{p}}{k_{\infty}},\ Le=\frac{\alpha^{*}}{D_{B}}\ ,\ s1=\frac{b_{1}}{b},\ M=\frac{\sigma B_{0}^{2}}{\rho a},\\ N_{T} &= \frac{\lambda_{1}D_{T}(Tw-T_{0})}{T_{\infty}\nu},\ N_{B}=\frac{\lambda_{1}D_{B}(C_{w}-C_{0})}{\nu}\end{aligned} \tag{16}$$

Skin friction coefficient is as follows:

$$C_{f}=\frac{\tau_{w}}{\rho U_{w}^{2}}, \tag{17}$$

where, shear stress τ_w is given by

$$\tau_{w}=\mu\left[1-\frac{\beta^{2}}{c}\left(\frac{\partial u}{\partial y}\right)\Big|_{y=0}\right]^{n}\left(\frac{\partial u}{\partial y}\right)\Big|_{y=0}. \tag{18}$$

In non-dimensional form:

$$C_f \sqrt{\mathrm{Re}_x} = \left[1 - \frac{\alpha}{6} f''(0)\right]^n f''(0). \tag{19}$$

Defining Nusselt number as:

$$Nu = \frac{-xk \left(\frac{\partial T}{\partial y}\right)\Big|_{y=0}}{k\left(T_w - T_\infty\right)}. \tag{20}$$

In dimensionless variables, we have

$$\frac{Nu}{\sqrt{\mathrm{Re}_x}} = -\left(\frac{1}{1-s1}\right)\theta'(0), \tag{21}$$

where $\mathrm{Re}_x = \frac{ax^2}{\nu}$ represents the local Reynolds number.

3 Solutions Method

The developed equations are non-linear in character and, thus, difficult to acquire exact solutions. It is therefore suitable to employ analytical approximate technique termed as HAM to solve them. To this end, we define initial approximation and linear operator by the relations:

$$f_0(\eta) = 1 - \exp(-\eta), \tag{22}$$

$$\theta_0(\eta) = \exp(-\eta) - s1\exp(-\eta), \tag{23}$$

$$\varphi_0(\eta) = -\frac{N_T}{N_B}(1-s1)\exp(-\eta), \tag{24}$$

$$\mathcal{L}_f(f) = \frac{d^3 f}{d\eta^3} - \frac{df}{d\eta},\ \mathcal{L}_\theta(\theta) = \frac{d^2\theta}{d\eta^2} - \theta,\ \frac{d^2\varphi}{d\eta^2} - \varphi, \tag{25}$$

with

$$\mathcal{L}_f\left[A_1 + A_2 e^{\eta} + A_3 e^{-\eta}\right] = 0, \tag{26}$$

$$\mathcal{L}_\theta\left[A_4 e^{\eta} + A_5 e^{-\eta}\right] = 0, \tag{27}$$

$$\mathcal{L}_\varphi\left[A_6 e^{\eta} + A_7 e^{-\eta}\right] = 0, \tag{28}$$

where, A_i $(i = 1 - 7)$ represent arbitrary constants.

Generally analytical solutions are

$$f_m(\eta) = f_m^{\star}(\eta) + A_1 + A_2 e^{\eta} + A_3 e^{-\eta}, \tag{29}$$

$$\theta_m(\eta) = \theta_m^{\star}(\eta) + A_4 e^{\eta} + A_5 e^{-\eta}, \tag{30}$$

$$\varphi_m(\eta) = \varphi_m^{\star}(\eta) + A_6 e^{\eta} + A_7 e^{-\eta},$$

in which $f_m^{\star}(\eta), \theta_m^{\star}(\eta)$ and $\varphi_m^{\star}(\eta)$ represents special solutions.

3.1 Convergence analysis

The $\hbar_f$, $\hbar_\theta$ and $\hbar_\varphi$ represent auxiliary parameters for $f(\eta), \theta(\eta)$ and $\varphi(\eta)$, respectively. The said parameters play impactful role in controlling and managing the convergence of consequent series solution. To achieve the suitable values of these variables, $\hbar$-curves have been sketched in Fig. 2. It is noticeable that the permissible ranges are $-1.8 \leq \hbar_f \leq -0.4$, $-1.7 \leq \hbar_\theta \leq -0.5$ and $-1.6 \leq \hbar_\varphi \leq -0.7$.

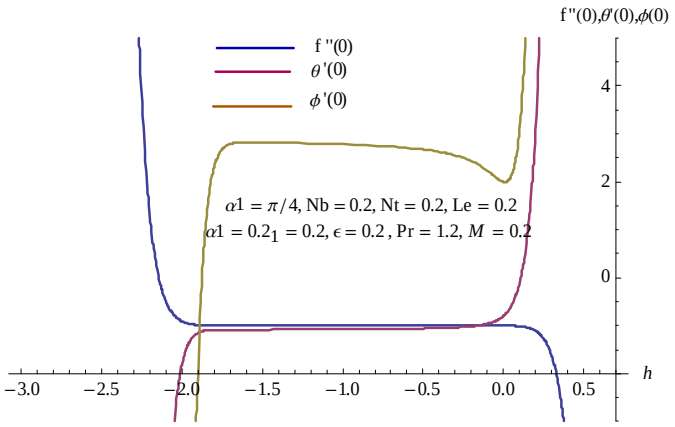

Fig. 2 h-curves for $f(\eta), \theta(\eta)$ and $\varphi(\eta)$

4 Discussion

In this portion, behavior of the eminent parameters is investigated on the velocity, temperature and nanofluid concentration for two values of power law index $n = 1$ and $n = 2$. Fig. 3 has been traced to understand the variation of fluid parameter (α) on the velocity distribution for both values of n. It is reflected from this figure that the magnitude of the velocity declines with increment in the fluid parameter α. Physically, for higher α, fluid viscosity decays and as a consequence, the velocity field decrements. The velocity gradient for diverse values of inclination angle $\alpha 1$ and for two values of n is displayed in Fig. 4. Velocity gradient curve decays for larger $\alpha 1$. In fact, dominant angle $\alpha 1$ increments magnetic field which consequently produces higher Lorentz force. That is why velocity field declines. Fig. 5 is drawn to display the influence of Hartmann number M on velocity gradient for fixed values of power law index n.It can be seen that velocity reduces for higher Hartmann number M. Physically, Lorentz force enhances for dominant Hartmann number. Thus, velocity reduces. Fig. 6 displays the variation of thermal conductivity parameter ϵ on temperature. For larger ϵ, temperature grows. Physically, higher ϵ intensifies the thermal conductivity and resultantly, temperature enhances for both values of n. Features of Prandtl number (Pr) on fluid temperature curve are addressed in Fig. 7. Enlargement in Prandtl number shows decaying behavior of temperature field. Greater Prandtl number is accountable for less thermal diffusivity. Thus, lesser heat transfers from heated surface to cold surrounding fluid. Hence, temperature decays for fixed n. Fig. 8 depicts the features of Nt thermophoresis parameter on temperature field. Temperature rises for thermophoresis phenomenon because particles are pushed to the cold region from heated one, therefore, temperature field enhances for both values of n. Fig. 9 shows the variation in temperature field by thermal stratification parameter $s1$. Higher intensity of $s1$ reduces temperature distribution. Physically, higher thermal stratification produces

significant density difference between the upper and lower parts of the fluid which further reduces the convective flow. Thus, temperature field decays for fixed n. Fig.10 depicts the temperature field under associated boundary layer for diverse values of Brownian parameter. As Nb grows, temperature enhances for both values of n. Bodily an enlargement in Nb reacts in the demotion of mean assimilation coefficient which is accountable for the improvement of temperature distribution. Fig. 11 shows the impact of Lewis number Le on concentration. Physically, mass transfer reduces by increasing Lewis number Le. As a result concentration field decays for fixed n. Fig. 12 describes the behavior of Brownian parameter Nb on fluid concentration. The concentration field is decaying function of Brownian parameter Nb. In fact, when Brownian parameter grows, the collisions between fluid particles enhances and ensures lower mass transport phenomenon from heated sheet towards cold fluid. Therefore, concentration field shows decreasing behavior for fixed n. Fig. 13 reflects the behavior of thermophoresis parameter Nt on fluid concentration. Incriementing behaviour of concentration is noted for dominant Nt for both values of n. Fig. 14 illustrates the behavior of M and α on coefficient of skin friction. Magnitude of skin friction rises for both M and α. Fig. 15 depicts the behavior of Pr and $s1$ on rate of heat transfer. Clearly Nusselt number shows dominating result for Pr and $s1$.

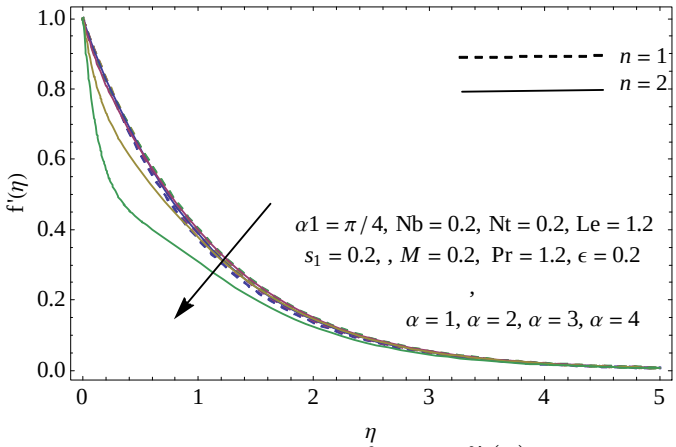

Fig. 3 Impact of α on $f'(\eta)$

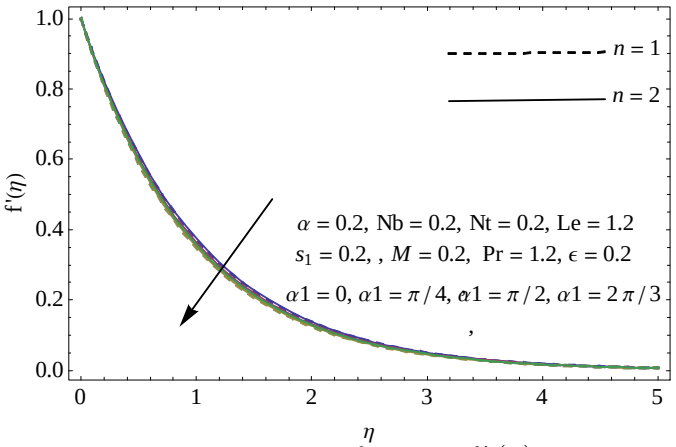

Fig. 4 Impact of $\alpha 1$ on $f'(\eta)$

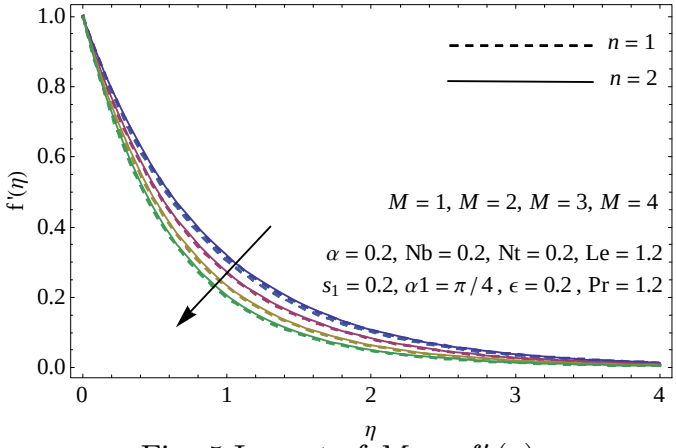

Fig. 5 Impact of M on $f'(\eta)$

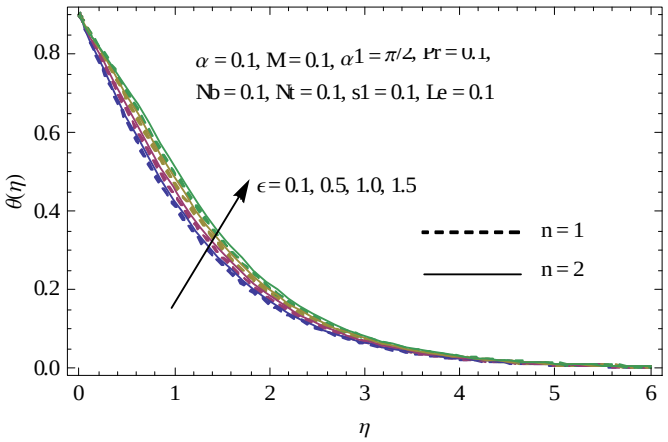

Fig. 6 Impact of ϵ on $\theta(\eta)$

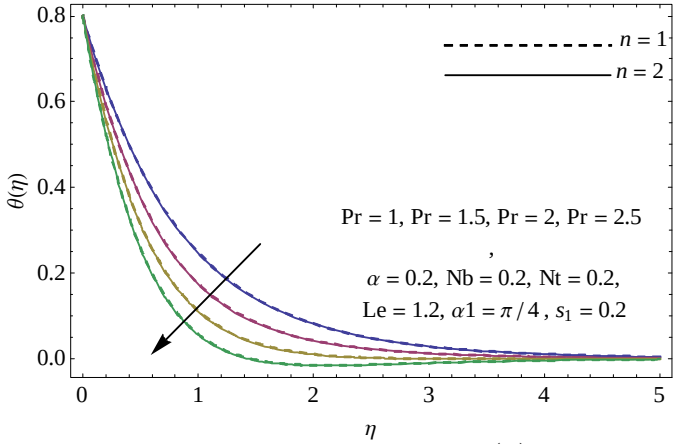

Fig. 7 Impact of Pr on $\theta(\eta)$

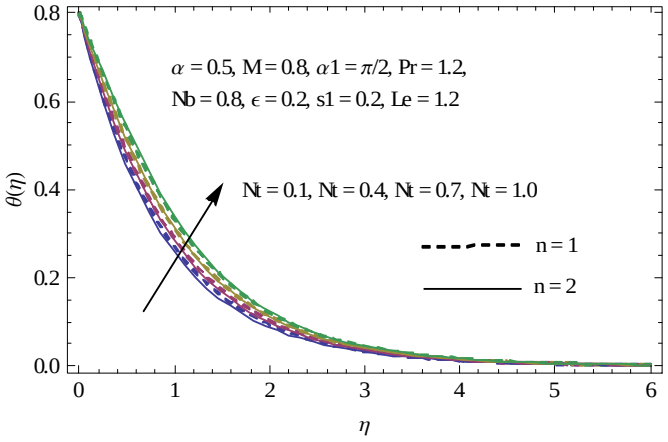

Fig. 8 Impact of Nt on $\theta(\eta)$

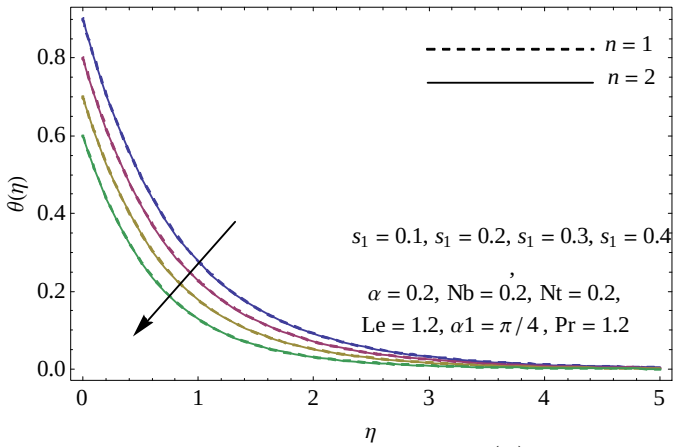

Fig. 9 Impact of $s1$ on $\theta(\eta)$

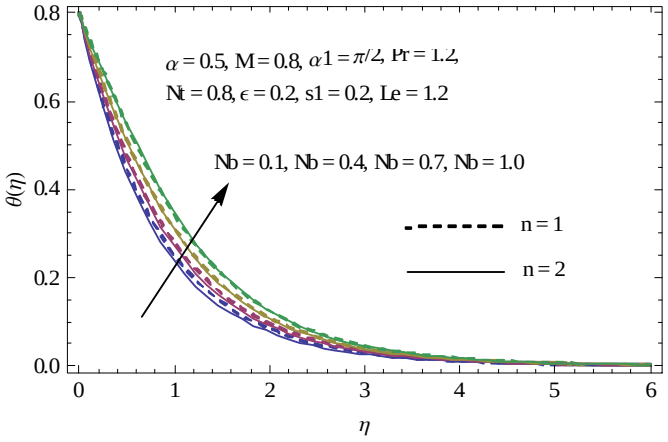

Fig. 10 Impact of Nb on $\theta(\eta)$

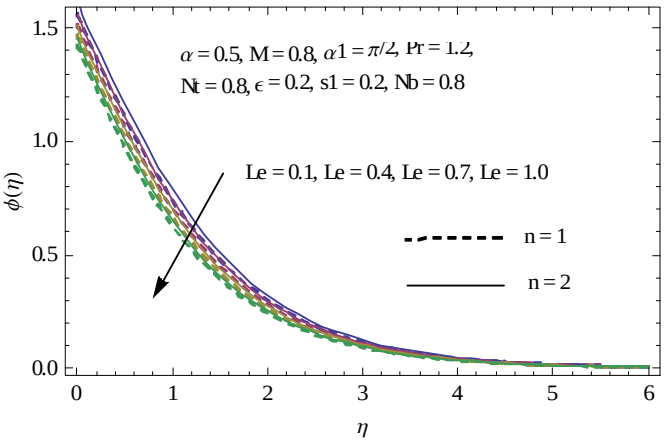

Fig. 11 Impact of Le on $\varphi(\eta)$

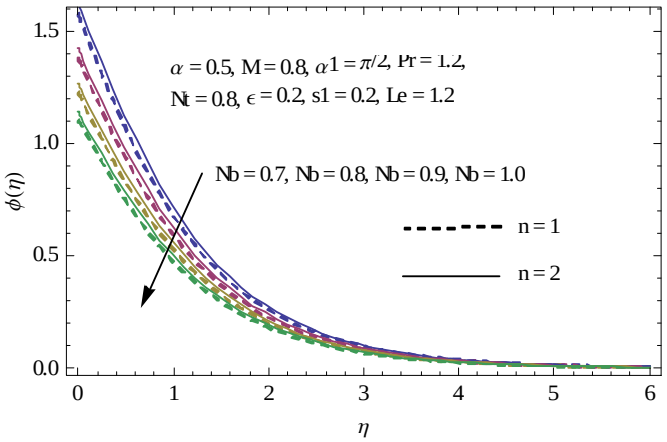

Fig. 12 Impact of Nb on $\varphi(\eta)$

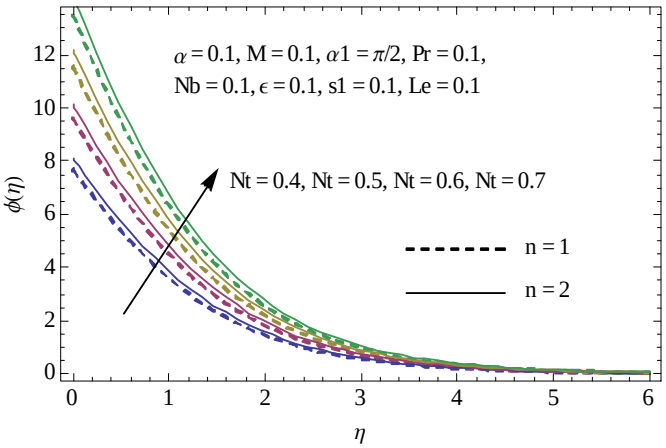

Fig. 13 Impact of Nt on $\varphi(\eta)$

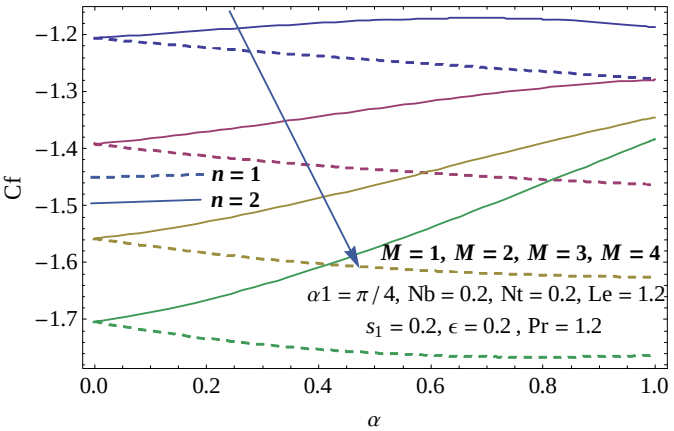

Fig. 14 Impact of M & α on Cf

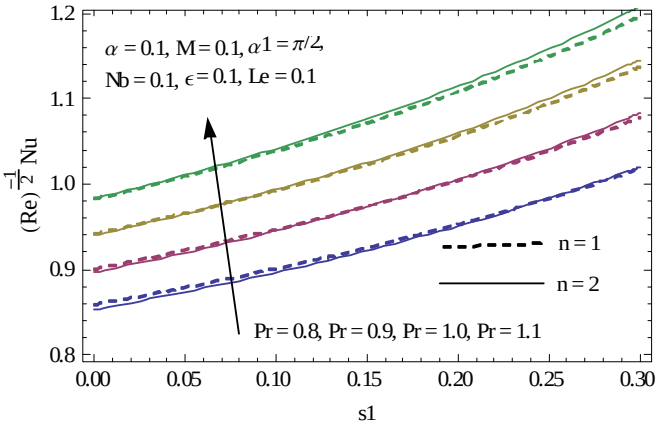

Fig. 15 Impact of Pr & $s1$ on Nu

5 Closing remarks

Characteristics of Sutterby nanofluid over a linearly stretchable plate with inclined MHD, linear stratification and varying thermal conductivity in the presence of zero flux condition have been disclosed in this attempt. The following key points are worth mentioning.

- Decaying behavior of velocity field is achieved for higher Hartmann number.
- Higher thermal conductivity parameter ϵ intensifies the thermal distribution.
- Temperature profile decays for higher stratified parameter $s1$.
- Brownian motion and thermophoresis parameters result in increment of temperature field.
- Brownian parameter is decreasing function for concentration field whereas concentration grows for higher thermophresis parameter.

References

[1] Choi, S. U., & Eastman, J. A. (1995). Enhancing thermal conductivity of fluids with nanoparticles (No. ANL/MSD/CP-84938; CONF-951135-29). Argonne National Lab., IL (United States).

[2] Prasad, P. D., Kumar, R. K., & Varma, S. V. K. (2018). Heat and mass transfer analysis for the MHD flow of nanofluid with radiation absorption. Ain Shams Engineering Journal, 9 (4), 801-813.

[3] Tian, X. Y., Li, B. W., & Hu, Z. M. (2018). Convective stagnation point flow of a MHD non-Newtonian nanofluid towards a stretching plate. International Journal of Heat and Mass Transfer, 127, 768-780.

[4] Ahmed, J., Khan, M., & Ahmad, L. (2019). Stagnation point flow of Maxwell nanofluid over a permeable rotating disk with heat source/sink. Journal of Molecular Liquids, 287, e110853.

[5] Khan, M. I., Kumar, A., Hayat, T., Waqas, M., & Singh, R. (2019). Entropy generation in flow of Carreau nanofluid. Journal of Molecular Liquids, 278, 677-687.

[6] Derakhshan, R., Shojaei, A., Hosseinzadeh, K., Nimafar, M., & Ganji, D. D. (2019). Hydrothermal analysis of magneto hydrodynamic nanofluid flow between two parallel by AGM. Case Studies in Thermal Engineering, 14, e100439.

[7] Hamid, A., & Khan, M. (2018). Unsteady mixed convective flow of Williamson nanofluid with heat transfer in the presence of variable thermal conductivity and magnetic field. Journal of Molecular Liquids, 260, 436-446.

[8] Hayat, T., Qayyum, S., Alsaedi, A., & Ahmad, B. (2018). Mechanisms of double stratification and magnetic field in flow of third grade fluid over a slendering stretching surface with variable thermal conductivity. Results in physics, 8, 819-828.

[9] Salawu, S. O., Kareem, R. A., & Shonola, S. A. (2019). Radiative thermal criticality and entropy generation of hydromagnetic reactive Powell–Eyring fluid in saturated porous media with variable conductivity. Energy Reports, 5, 480-488.

[10] Ahmed, J., Khan, M., & Ahmad, L. (2019). MHD swirling flow and heat transfer in Maxwell fluid driven by two coaxially rotating disks with variable thermal conductivity. Chinese Journal of Physics, 60, 22-34.

[11] Khan, M. I., Hayat, T., Khan, M. I., Waqas, M., & Alsaedi, A. (2019). Numerical simulation of hydromagnetic mixed convective radiative slip flow with variable fluid properties: a mathematical model for entropy generation. Journal of Physics and Chemistry of Solids, 125, 153-164.

[12] Bilal, S., Alshomrani, A. S., Malik, M. Y., Kausar, N., & Khan, F. (2018). Analysis of Carreau fluid in the presence of thermal stratification and magnetic field effect. Results in Physics, 10, 118-125.

[13] Anjum, A., Mir, N. A., Farooq, M., Khan, M. I., & Hayat, T. (2018). Influence of thermal stratification and slip conditions on stagnation point flow towards variable thicked Riga plate. Results in Physics, 9, 1021-1030.

[14] Khan, M., Malik, M. Y., Salahuddin, T., Saleem, S., & Hussain, A. (2019). Change in viscosity of Maxwell fluid flow due to thermal and solutal stratifications. Journal of Molecular Liquids, 288, 110970.

[15] Hamid, A., Hashim, Alghamdi, M., Khan, M., & Alshomrani, A.S. (2019). An investigation of thermal and solutal stratification effects on mixed convection flow and heat transfer of Williamson nanofluid. Journal of Molecular Liquids, 284, 307-315.

[16] Ali, A., Nazir, M., Awais, M., & Malik, M. Y. (2019). Stratification phenomenon in an inclined rheology of UCM nanomaterial. Physics Letters A, 383(18), 2201-2206.

[17] Liao, S. (2012). Homotopy analysis method in nonlinear differential equations (pp. 153-165). Beijing: Higher education press.

[18] Hayat, T., Ali, S., Awais, M., & Obaidat, S. (2013). Stagnation point flow of Burgers' fluid over a stretching surface. Progress in Computational Fluid Dynamics, an International Journal, 13(1), 48-53.

[19] Hayat, T., Ali, S., Awais, M., & Alhuthali, M. S. (2015). Newtonian heating in stagnation point flow of Burgers fluid. Applied Mathematics and Mechanics, 36(1), 61-68.

[20] Ahmad, S., Farooq, M., Javed, M., & Anjum, A. (2018). Double stratification effects in chemically reactive squeezed Sutterby fluid flow with thermal radiation and mixed convection. Results in Physics, 8, 1250-1259.

[21] Anjum, A., Mir, N. A., Farooq, M., Javed, M., & Ahmad, S. (2019). Investigations of Viscous Dissipation in Stagnation Point Flow Past a Stretchable Riga Wall: Modern Analysis of Heat Transport. Communications in Theoretical Physics, 71(4), 377.